Accepted Manuscript

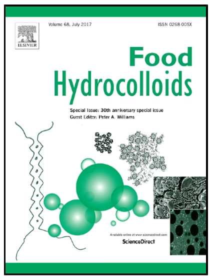

Tribo-Rheology and Sensory Analysis of a Dairy Semi-Solid

Fernanda C. Godoi, Bhesh R. Bhandari, Sangeeta Prakash

PII:	S0268-005X(16)31036-0
DOI:	10.1016/j.foodhyd.2017.04.011
Reference:	FOOHYD 3859
To appear in:	*Food Hydrocolloids*
Received Date:	11 January 2017
Accepted Date:	06 April 2017

Please cite this article as: Fernanda C. Godoi, Bhesh R. Bhandari, Sangeeta Prakash, Tribo-Rheology and Sensory Analysis of a Dairy Semi-Solid, *Food Hydrocolloids* (2017), doi: 10.1016/j.foodhyd.2017.04.011

RESEARCH HIGHLIGHTS

- Tribo-rheology of a dairy semi-solid model, custard
- Effect of starch, carrageenan and fat on the flow behaviour, lubricant properties and particle size distribution
- Insights on determination of tribological regimes in friction curves: coefficient of friction vs sliding speed
- It was suggested that tribology mechanisms are mainly influenced by hydrophobic interactions and selective entrainment based on particle size
- Sensory evaluation of bulk-related attributes well correlated to viscosity measurements; however no sensitive perception of fat-related attributes was observed.

TRIBO-RHEOLOGY AND SENSORY ANALYSIS OF A DAIRY SEMI-SOLID

Fernanda C. Godoi[1]; Bhesh R. Bhandari[1] and Sangeeta Prakash[1]*

[1] The ARC Dairy Innovation Hub, The University of Queensland, Brisbane 4072, Australia.

***Corresponding author:**

Dr Sangeeta Prakash

s.prakash@uq.edu.au

School of Agriculture and Food Sciences

Hartley Teakle Building, Room C406

The University of Queensland

Brisbane QLD 4072

Abstract

Tribology science is devoted on explaining the friction behaviour of interacting surfaces in relative motion. Several tribological systems have been used to measure coefficient of friction (CoF) vs sliding speed of entrained food layer between two rubbing surfaces. These results can be correlated with fat-related attributes perceived during oral processing. This study aims to investigate the effect of starch, carrageenan and fat on the friction profile; flow behaviour and particle size distribution. Friction curves were obtained for custards using a tribo-rheometer with a rotating metallic geometry rubbing the surface of 3M tape with roughness similar to that depicted by human tongue. Confocal Laser Scanning Microscopy (CLSM) images of custard collected during friction experiment helped to explain the characteristics of tribological regimes. As expected, fat-containing samples depicted remarkably lower CoF than skim compositions (fat: 0.2<CoF<0.08 and skim: 0.6<CoF<0.3). The presence of fat not only influenced CoF magnitude but the establishment of tribological regimes (TRs). Fat-custards depicted three TRs, assigned as: (1) fluid entrainment (decreasing-CoF), (2) gel particle entrainment (increasing-CoF) and (3) accumulation of multi-layers of material at high speeds (decreasing or sometimes constant-CoF). Skim–samples, however, presented a prolonged decreasing CoF over the sliding speed range tested. Conversely to tribo-rheological results, sensory analysis revealed lack of hydrocolloid effect on the perception of fat-related attributes. This was assigned to the presence of saliva facilitating the food microstructure breakdown. We emphasize that our tribological study focused on the friction trend; future experiments will involve the use of saliva to explain the mechanisms of food oral processing.

Key-words: rheology, tribology, sensory, dairy semi-solid.

1. INTRODUCTION

Semi-solid foods usually consist of complex gel networks made of proteins or carbohydrates (polysaccharides) with high or low fat content. Oral processing of semi-solids requires minimum mastication efforts because they already resemble the bolus formed for swallowing (de Wijk, Prinz, Engelen, & Weenen, 2004; Engelen, et al., 2003). At the first stage of food ingestion in the mouth a thick layer of product is present between the surface of tongue and palate and rheological behavior plays an important role on the perception of thickness. As a subsequent step, microstructure break-down of the food entrapped between tongue and palate takes place by the action of enzymes present in saliva, shear forces and sliding speeds.

Hydrocolloids (proteins and carbohydrates) are known by their ability of attracting water molecules and entrapping fat which justify their intense use as texture modifiers in food. Improvements on the oral perception, for example, of creaminess and thickness relies on the mechanism of entrapped fat migration from inner regions of the semi-solid network to surfaces of tongue and palate under friction by the sliding movements of tongue (de Wijk & Prinz, 2007; de Wijk, et al., 2004; Engelen, et al., 2003). Researchers have successfully associated bulk-related sensory attributes, such as thickness, with flow behavior and viscoelastic properties determined by means of rheological methods. However, fat-related attributes like creaminess and oiliness cannot be fully assigned to rheological behavior. For this reason, the combined study of tribology and rheology has been suggested as a promising alternative to explain oral perception (Chen, Liu, & Prakash, 2014; Liu, Stieger, van der Linden, & van de Velde, 2015; Malone, Appelqvist, & Norton, 2003; Nguyen,Bhandari & Prakash, 2016; Nguyen, Nguyen, Bhandari & Prakash, 2015; Pradal & Stokes, 2016; Prakash, Tan, & Chen, 2013).

Classical tribology which is the study of friction behaviour of Newtonian isotropic lubricants has been applied, with adaptations, to understand the lubricant properties of food multicomponent systems. In classical tribology, the general lubrication trend is explained by the Stribeck curve consisting of a plot of coefficient of friction (CoF) versus the dimensionless lubrication parameter Λ, which is defined by relation between dynamic viscosity η_d [N s m^2], sliding speed ν [mm s^{-1}] and normal load force projected on the geometrical surface [N m^{-1}] (Eq. 1).

$$\Lambda = \frac{\eta_d \times \nu}{F_N} \quad (1)$$

Three regimes can be distinguished from the classical Stribeck curve, they are named: (1) boundary, (2) mixed and (3) hydrodynamic. The boundary regime is typically observed at low speeds and the friction is mainly generated by the interaction between the two rubbing surfaces (severe wear). As the sliding speed increases, the entrained lubricant reduces the contact of the surface roughness, until the limiting condition of fully separated surfaces is reached; this phase is assigned as mixed regime. Subsequently, further increase in speed causes an increase in the friction coefficient, which relies on the internal friction of the lubricant fluid (resistance to flow) (Gohar & Rahnejat, 2008).

Food Tribology is an emerging research area focused on understanding the lubrication between tongue and palate in the presence of a thin layer of food experiencing sliding speeds ranging from 1 to 50 mm s^{-1} (Chojnicka-Paszun, de Jongh, & de Kruif, 2012; Malone, et al., 2003). Many efforts have been devoted to mimic the environment conditions of the mouth in tribo-rheological apparatus, including temperature control (generally maintained at 35-37 °C) and injection of saliva on the surface of the substrate (Selway & Stokes, 2013) which must present roughness similar to that observed by the tongue (Nguyen, Nguyen, Bhandari, & Prakash, 2015). The use of saliva, however, cannot assure complete sensory correlation as it is produced as part of a dynamic process during oral processing. Moreover, the composition of human saliva is variable among individuals (Chiappin, Antonelli, Gatti, & De Palo, 2007) which compromises the efficacy of using artificial saliva for this kind of study.

Thus, finding the correlation between sensory attributes and tribo-rhelogical results is an exciting but still unsolved problem. The deep understanding about tribological regime is essential before achieving correlation with sensory. As an example, Selway and Stokes (2013) investigated the effect of fat content on commercial samples of custards and yogurt in the rheology and tribology profile. Another interesting work was conducted by Liu, Stieger, van der Linden, & van de Velde (2015) where sensory profile was correlated with tribological and rheological behavior of emulsion-filled gels as models for semi-solid and solid foods. They have used Confocal Laser Scanning Microscopy (CLSM) to capture differences in the microstructure after submitting the product to shear in an Optical tribological configuration (OCT). Their edible system was prepared with non-dairy fat from various sources (beef, pork and poultry), surfactants (Tween 20, whey protein isolate) and pork gelatin as gel matrix. Laguna et al. (2017) have recently shown that typical Stribeck curves presented different sensitivity to fat content for dairy liquid and semi-solids. The friction curves were not successful in discriminating whole and skim milk in presence of artificial saliva. Conversely, the curves were effective in differentiating the fat content of yoghurt and cheese for experiments conducted with and without saliva.

Although Stribeck analysis has been widely reported in the study of food-related products; Gabriele, Spyropoulos & Norton (2010) have reported that the dependence of friction on increasing sliding speed ramp for fluid gels composed of agarose could not be analyzed in terms of classical tribology. They proposed a mechanism of fluid gel lubrication which divides the friction curves in three zones: Zone A, at low sliding speed, only the fluid medium can be entrained into the gap formed between ball and the disk (decreasing CoF trend); Zone B, represented by the entrainment of the particles (increasing CoF trend) and Zone C where the sliding speed is high allowing more particles in the gap and CoF depicts a decreasing trend again as the magnitude of the gap is higher than the size of the entrained particles. The rich literature reporting about tribology of fluids and gels which are commonly used as emulsifiers and thickener agents helps to understand the mechanisms of friction represented by real multicomponent food systems (Fernández Farrés & Norton, 2015; Gabriele, Spyropoulos, & Norton, 2010; Garrec & Norton, 2013; Malone, et al., 2003; Moakes, Sullo, & Norton, 2015).

In this research, we investigated the combined effect of essential ingredients (starch, κ-carrageenan and fat) on the friction behavior of custard desserts. A simple tribo-rheometer set-up (Nguyen,Bhandari & Prakash, 2016; Nguyen, Nguyen, Bhandari & Prakash, 2015) was used to evaluate the friction behavior. Depending on the product tested, this device can perform friction measurements at sliding speeds up to 1000 mm s^{-1}. For less viscous materials, such as chocolate milk, a threshold sliding speed is observed at 50 mm s^{-1} when friction sound can be heard, due the vibration caused by micro-impact of the two rubbing surfaces.

Our findings were focused on the description of tribological regimes without the use of saliva as lubricant agent of the substrate surface. CLSM images were taken at the turning points of the identified tribo-regimes to support our hypothesis of selective particle/fluid entrainment within the gap formed between the geometry and substrate surface by increasing sliding speed. Sensory analysis was conducted to reveal whether the panelists were able to discriminate the samples based on the concentration of fat, starch and κ-carrageenan. The sensitivity of sensory analysis was compared with the one obtained by rheology and tribology experiments by showing different trends and magnitudes according to the formulation tested. It is worth mentioning that tribo-rheological experiments mimic the food oral processing only in terms of temperature, shear range and roughness of the substrate (3M tape).

2. MATERIALS AND METHODS

2.1 Materials

Custard formulations were prepared in the laboratory using skim milk powder purchased from Total Foodtec Pty ltd.; natural vanilla extract (Queen Fine Foods, Australia), caster sugar and pure cream (Parmalat, Australia) from local markets. Other ingredients such as, modified tapioca starch (product code: Kreation 440), κ-Carrageenan (product code: MV306) and sodium hexametaphosphate (product code: 65 Food Grade) were provided by IMCD-Australia.

2.2 Custard preparation

Custard dessert formulations were prepared as follows. At first, skim milk powder was hydrated in water for 3 hrs using an overhead propeller stirrer at 1200 rpm. Afterwards, caster sugar, hexametaphosphate, thickener agent (κ-Carrageenan) and cream were incorporated to the mixture which was transferred to a water bath (T = 95 ºC) and held under constant stirring for 15 minutes. Then, pre-gelatinized starch was poured into the mixture which remained in the water bath for 30 min. Vanilla flavor was added to the composition 5 min before the completion of cooking. The thermo-reversible gels formed after subsequent cooling at room temperature were disrupted and homogenized using a Multimix™ high-shear mixer (HSM 2003 SV/SLI).

A central composite design (CCD) containing a 2^3 factorial design with 3 center points was performed to estimate the effects of starch (ST), κ-Carrageenan (κCar) and fat (F) on the particle size distribution and rheological behavior of the custard dessert formulations. The tested concentrations of starch, κCar and fat are described in **Table 1**. The content of skim milk powder (10% w/w), caster sugar (4.5% w/w), Vanilla flavor (1% w/w) and sodium hexametaphosphate (0.1% w/w) were kept constant.

Table 1

2.3 Laser scattering

Laser scattering technique was performed for measuring the particle size distribution of each custard sample. A Mastersizer 2000 (Malvern Instruments, Worcestershire, UK) was used for the measurements; assuming a regular spherical shape of the particles (Mie Scattering Principle) (Malvern-Instruments, 2007a). The refractive index of the material and dispersant was, respectively, 1.46 (milk-fat) and 1.33 (water) (Malvern-Instruments, 2007b). Volume mean diameter ($D_{4,3}$) was considered as dependent variable of the factorial design.

2.4 Rheological and tribological measurements

All samples were equilibrated at room temperature (22 - 25°C) for 1 hour prior to rheological and tribological measurements which were performed at 35°C to simulate the oral condition.

2.4.1 Rheological and tribological measurements

Rheometer set-up

Steady state and dynamic measurements were conducted with an AR-G2 rheometer (TA Instruments, USA) at 1000 μm gap using 40 mm stainless steel sandblasted geometry (surface roughness of 4 ± 2 μm). A solvent trap cover and solvent trap geometry partially filled with distilled water were used to maintain a thermally stable vapour barrier and avoid sample evaporation during the experiments.

Steady state and dynamic operational procedure

For the steady state shear measurements, a shear rate ranging from 0.1 to 1000 s^{-1} was applied with acquisition rate of 10 points per decade. Since shear rates ranging from 10 to 100 s^{-1} demonstrate a correlation for chewing and swallowing of foods (Shama & Sherman, 1973), the apparent viscosity at 50 s^{-1} was used as a parameter of comparison among samples. Dynamic experiments were conducted for semi-solid samples only within the linear viscoelastic range (LVR) running a frequency sweep small enough to avoid the collapse of the structure (strain 0.01%). Storage modulus (G') and the loss modulus (G'') were recorded over the range ω=1-100 rad s^{-1} of angular frequency.

2.4.2 Tribological measurements

Tribo-rheometer set-up

Tribological tests were performed on a Discovery Hybrid Rheometer (TA Instruments, USA) to evaluate the lubricant properties of each custard formulation, as described elsewhere (Nguyen,Bhandari & Prakash, 2016; Nguyen, Nguyen, Bhandari & Prakash, 2015). **Fig. 1** illustrates the tribo-rheometer configuration which consists of a ring on plate geometry coupled to a rheometer head through coupling adapter and beam coupling to perform rotation movement. The ring's dimensions allows for a well-defined contact surface permitting the computation of the friction and normal stress.

Figure 1

Solid substrate (3M Transpore Surgical Tape 1527-2) with known surface roughness and well depth (R_a = 31.5 μm, well depth = 170 μm, respectively) was cut in a square shape, placed and fixed on top of the lower plate geometry before the measurement (Nguyen, Nguyen, Bhandari & Prakash, 2015). The choice of the substrate was based on the human tongue roughness ranging from 42-95 μm (Nagaoka, et al., 2001) and the heights of filiform and fungiform papillae within 200-300 μm and 100 μm, respectively (Ranc, Servais, Chauvy, Debaud, & Mischler, 2006).

Friction behavior operational procedure

Through preliminary tests, it was possible to determine the time and quantity of material necessary for each run. It is worth mentioning that the time applied during the tribological test cannot be related to the time of oral processing, but it is associated to the time required for reaching friction equilibrium at each sliding speed recorded. The amount of sample must be enough to cover the surface of the substrate with a thin film (~ 2 mm) of product. For custard, the recommended amount of material to spread over the surface of the substrate is 0.5 g. A practicable time of 10 min was adopted for all the experiments based on the reproducibility of the friction curves and absence of dried debris at the end of the run. The samples were spread over the surface of the substrate and a normal force of 2N was set by adjusting the gap between the surface and geometry. Conditioning step was performed by pre-shearing the samples at the rotational speed of 0.01 rad s^{-1} for 1 minute, and then they were equilibrated for another 1 minute before each measurement. Afterwards, increasing rotational speed (IRS) ramp was set from 0.01 to 6.5 rad s^{-1} with acquisition of 20 points per decade during 10 min of experiment. During the tribological test, the coefficient of friction (CoF) was determined as the ratio of friction stress (σ_F) to the normal stress (σ_N), described by **Eq. 2**, and plotted against the increasing sliding speed (**Eq. 3**) in log-log scale.

$$CoF = \frac{\sigma_F}{\sigma_N} = \frac{M}{F_N} \cdot \frac{(r_2 + r_1)}{(r_2^2 + r_1^2)} \quad (2)$$

Where M : torque [N m] and F_N : normal force [N].

$$v_s = \overline{R} \cdot \omega \quad (3)$$

Where v_s is the sliding speed [mm s^{-1}], $\overline{R}$ is the average between ring inner and outer radius (r_1 =14.5 mm and r_2 =16 mm) and ω is the controlled rotational speed [rad s^{-1}].

The friction curves (CoF vs sliding speed) were analyzed in terms of the following friction parameters: initial CoF (CoF_i), corresponding to CoF measured at 0.15 mm s^{-1}; minimum CoF (CoF_{min}) and peak height (*h*, observed only for certain samples) from the baseline built passing through CoF_{min} using the Peak Analyzer Tool of OriginLab© (version OriginPro 8.5) at second derivative mode.

2.5 Confocal laser microscopy (CLSM)

Staining was performed at ambient temperature. Except for nile red which was dissolved in PEG200 solution, all the dyes used were dissolved in distilled water at concentration of 0.01 g L^{-1}. Nile red (Sigma-Aldrich), fast-green FCF (Sigma-Aldrich), fluorescein-isothiocyanate FITC (Sigma-Aldrich) and calco-fluor white (Sigma-Aldrich) were used to label, respectively, fat, protein, starch and κCar. Equal proportions of the dyes were added to sample before tribological experiment (10 μL of dye mixture per g of sample). Stained custard was placed on the surface of the substrate and an increasing speed setting was programmed as described in **Section 2.4**. The rotating geometry was stopped at different stages of the friction curve (0.5, 2.5 and 10 mm s^{-1} of sliding speed) determined by the friction behavior results. Once the geometry was stopped, it was raised and the tape was removed for imaging of the friction area using a Diskovery Spinning Disk Confocal system (Nikon).

2.6 Contact angle measurement

Aiming to estimate the hydrophobicity of the 3M tape, the contact angle formed by sessile droplets of water and ethanol was measured using an OCA 15 EC/B Dataphysics GmbH (Germany). The drop was allowed to equilibrate on the substrate surface for a total of 30 seconds.

2.7 Sensory evaluation

Custard samples selected for sensory measurements are indicated in **Table 1** by asterisk symbols (*). Panelists were seated in sensory booths with appropriate ventilation and lighting. Two sessions were conducted according to the Ranking descriptive analysis (RDA) sensory method described in (Richter, de Almeida, Prudencio, & de Toledo Benassi, 2010):

- **Session I (attribute generation)**: all the samples were presented to the assessors simultaneously. They were asked to evaluate each sample and record all the perceived attributes related to texture. Upon evaluation of all samples, they were asked to give a list of descriptive terms. To prepare the panel for Session 2, the assessors were told to order the samples for intensity; e.g. least viscous to most viscous.

- **Session II (sample rating)**: a list of common attributes were generated from **Session I** and given to the same assessors. They were asked to rank the samples in order of intensity for each attribute. **Table 2** shows the textural descriptors and their definitions used in our study.

A maximum of 5 samples were served per session. Equal amounts of each sample were placed into 60 mL cups labelled with randomly selected 3-digit codes and equilibrated at room temperature for at least 1 h before consumption. Samples were served to panelists with mineral water for palate cleaning. Eleven panelists evaluated samples for predefined textural attributes (**Table 2**) using a quantitative scale with increasing score from 1 to 5. Friedman non-parametric analysis of variance was performed to detect differences in the perception of oral attributes. The analysis was conducted in Minitab 17 (Minitab Inc., Chicago).

The least significant difference (LSD) for rank sums was also used for comparison between two individual products. Samples whose rank sums differed by more than LSD calculated amount (**Eq. 6**) were considered significant different (Lawless, 2010).

$$LSD = 1.96 \cdot \sqrt{\frac{K \cdot J \cdot (J+1)}{6}} \qquad (6)$$

Where $J = 5$ and $K = 11$ which represent the number of products ranked and panelists, respectively. Hence, in this study, $LSD = 14.55$.

Table 2

2.8 Statistical analysis

Particle volume mean diameter ($D_{4,3}$), apparent viscosity measured at 50 s^{-1} shear rate (η_{50}) and the friction parameters (CoF_i, CoF_{min} and h) were presented as mean ± standard deviation (SD) of triplicate experiments. MiniTab 17 software was used to analyse the significance of differences between the values (where applicable) using Analysis of Variance (ANOVA) with Tukey's HSD (honest significant difference) post hoc test at family error rate 5 at 95% of confidence level.

3. RESULTS AND DISCUSSION

3.1 Particle size distribution

Particle size distribution of the custard formulations ST(1)_κCar(0.0)_F(0), ST(2)_κCar(0.15)_F(3) and ST(3)_κCar(0.30)_F(6) are depicted by **Fig. 2a, 2b** and **2c**, respectively. In absence of fat and κCar, custard exhibited a mono-modal distribution which was assigned to the dispersed swollen starch granules. Overall, bimodal distribution was predominant for samples containing fat and κCar. However, a small peak could be observed between 100 and 1000 μm for lower concentrations of κCar which was assigned to the partial coalescence of milk-fat droplets. The major population coincided with that seen for ST(1)_κCar(0.0)_F(0). The small population with particle sizes ranging from 2 to 10 μm was attributed to the presence of fat globules. These results are in agreement with previous observation for custard size distribution (Tarrega & Costell, 2006).

Table 3 describes the calculated volume mean diameter ($D_{4,3}$) for all custard samples prepared at the proposed conditions by the factorial design explained in **Section 2.2**. Sample ST(3)_κCar(0.3)_F(0) depicted an average size of 35.3 ± 0.9 μm which was not significant different from samples ST(1)_κCar(0.3)_F(0), ST(1)_κCar(0.3)_F(6) and ST(2)_κCar(0.15)_F(3). The average size observed for these samples are of higher magnitude than the 3M tape roughness, Ra = 31.5 μm, determined previously by Nguyen, Nguyen, Bhandari & Prakash (2015). This important information can explain the entrainment of particles at low speeds of the friction curves (to be discussed in details by **Section 3.4.1**). A clear view of the significant effects of starch, κCar and fat on $D_{4,3}$ is shown by the Pareto charts illustrated by **Fig. 3a**. By adding κCar, the average particle size increased as a result of small aggregated particles entrapped by the network formed between κCar and casein micelles. However, the combined effects of κCar and starch resulted in a decay of the average particle size. Probably, an increase in the concentration of these two ingredients reduces the formation of gel structures between κCar and casein and halts the development of aggregated particles. Negative effect was observed upon addition of fat which has lower size than that observed by starch granules in **Fig. 2a**.

Figure 2

Table 3

Figure 3

3.1 Flow curves of custard dessert

The Pareto's chart shown by **Fig. 3b** demonstrates that the linear effects of κCar, starch and the interaction between κCar and starch increased significantly the η_{50} values. This trend is in agreement with previous studies which show the ability of starch and polysaccharides, such as κCar, to act as thickener agents (Tarrega, et al., 2006; Toker, Dogan, Caniyilmaz, Ersöz, & Kaya, 2013). Carrageenans are widely used in dairy desserts due their gelling, thickening, and stabilizing properties. Their structures are characterized by a linear polysaccharide consisting of repeating disaccharide sequences containing α-D-galactopyranose) and β-D-galactopyranose linked through 1-C-3 and 1-C-4 positions, respectively. Among the common varieties of carrageenans (Kappa, Iota and Lambda), kappa possesses the stronger gelling ability followed by iota, which form soft gels in presence of potassium and calcium. Lamda does not form gel when dispersed in aqueous solution; it is used as thickener agent. Gelling types carrageenan contain a 3,6 anhydro bridge on the B unit which forces the carbohydrate backbone to flip from 4-C-1 to a 1-C-4 conformation. The generated helix conformation can form cross-link networks and gels (Necas & Bartosikova, 2013).

Fig. 3b also reveals that the interaction effects "κCar & fat" and "starch & fat" decreased the η_{50} values. This indicates that the interspersed fat throughout the κCar-starch network possesses the ability of reducing the gel strength. Similar behavior has been observed for different dairy semi-solid systems. As an example, Nguyen, Bhandari & Prakash (2016) observed a decrease in the strength of protein network as the fat content increased in cream cheese samples.

Fig. 4 shows that the rheological pattern in terms of the viscosity dependence against shear rate was influenced by the composition of starch, κCar and fat in the prepared custard desserts. A stronger pseudoplastic behavior was observed for the samples containing high levels of starch and κCar which is a common characteristic of semi-solid foods (McCarthy, 2003). Compositions low in starch and κCar (e.g., ST(1)_κCar(0.0)_F(6) and ST(1)_kCar(0.0)_F(0)) depicted apparent viscosity ranging from around 0.1 to 0.001 Pa s over the four decades of shear rate, which is within the range of liquid dairy products (Nguyen, Bhandari & Prakash, 2016).

Figure 4

3.2 Viscoelastic properties

Fig. 5 depicts the storage modulus (G') and loss modulus (G'') between two decades of the angular frequency axis. The majority of the custard formulations exhibited viscoelastic properties including both solid (elastic) and liquid properties (viscous). Addition of κCar produced a remarkable increase in both viscoelastic functions: G' and G''. Furthermore, formulations containing κCar depicted G'> G'' which characterizes gel-like behavior. A clear effect of κCar, fat and starch concentrations on the viscoelastic properties was observed by calculating the loss factor equation ($G''/G' = tan\,\delta$) at an angular frequency of 10 rad s^{-1} (**Table 4**). As described by **Table 4**, no significant difference was observed on the gel strength upon addition of fat to the custard formulation.

Figure 5

Table 4

3.3 Friction curves of custard dessert

By allowing a product to be entrained between two rubbing surfaces friction loss and/or gain can be observed depending on the ability of the material to deposit on the static surface at different speeds. Conditions that facilitate the material entrainment, such as, particle size smaller than the surface roughness and interactions forces within functional groups of material and tape will reduce friction by preventing the dry contact between the two rubbing surfaces. The mechanisms of product entrainment in the gap formed between the rubbing-surfaces of the tribo-pair can be explained by measuring CoF from a condition of dry-contact (very low sliding speed) to high sliding speeds.

Fig. 6 shows four pairs of friction curves (with and without fat) grouped according to their composition of starch and κCar where: ST(1)_κCar(0.30), ST(1)_κCar(0.0), ST(3)_κCar(0.30) and ST(3)_κCar(0.0) sets are depicted by **Figs. 6a** to **6d**, respectively. As can be seen, the trend presented by the friction data differed widely in shape from Classical Stribeck curves which is characterized by a decrease in friction during ramp-up sliding speed experiments, followed by a minimum CoF as the hydrodynamic regime is activated. Despite this, our study enabled to discern broad patterns in the CoF measures, both across two main groups (with and without fat) and over long stretches of sliding speed.

Figure 6

Fig. 7 illustrates a schematic representation of the friction behaviour exhibited by non-fat and fat-containing samples. The friction parameters indicated by the arrows in **Fig. 7** are described in **Table 3**; they correspond to CoF measured at 0.15 mm s^{-1} (CoF_i), minimum CoF (CoF_{min}) and peak height from the baseline shown as dashed line (*h*). The last two parameters were determined by creating a baseline and finding peaks using the Peak Analyzer Tool of OriginLab© (version OriginPro 8.5) at second derivative mode. As expected, non-fat samples presented higher CoF values (see **Table 3**, non-fat samples showed CoF_i ~ 0.57 and CoF_{min} ~ 0.34; while fat-containing samples depicted CoF_i = 0.20 to 0.13 and CoF_{min} ~ 0.12) over the sliding speed range investigated. Interestingly, non-fat and fat-containing samples were different not only in magnitude but in friction behaviour against sliding speed.

Figure 7

The friction profile of non-fat samples was characterized by a decreasing CoF trend until CoF_{min} at around 10 mm s^{-1}. It is worth mentioning that, although the addition of κCar (0 to 0.3% w/w) and starch (from 1 to 3% w/w) caused an increase in viscosity for free-fat samples (as illustrated by flow curves, **Fig. 4**), the friction behavior in absence of fat was slightly influenced by κCar and starch. It is believed that, for non-fat samples, the mechanisms governing product entrainment in the decreasing CoF zone are not strongly dependent on hydrophobic interactions, as per the absence of fat. Probably, it mostly relies on the selective entrainment of liquid and/or particles of smaller size than the magnitude of the tape roughness which defines the gap formed between the tape and tribo-geometry as the sliding speed increases.

The friction behaviour of fat-containing samples, however, is more likely to be associated with hydrophobic interactions between the entrained product and the substrate surface. The 3M tape used in this study as substrate is made of polyester-rayon blend which naturally shows hydrophobic and hydrophilic sites, from polyester and rayon (regenerated cellulose fiber), respectively. As described by **Table 5** the comparison between the contact angle formed by a sessile droplet of water (most polar solvent) and ethanol reinforces the predominant hydrophobic characteristic of the material which composes the substrate. The prevailing non-polar sites lead to hydrophobic interactions with the emulsified fat droplets, forming a lubricant film on the surface of the tape (see **Fig. 7**).

Table 5

Fig. 7 clearly shows that fat-containing samples depicted CoF_{min} much earlier in the friction curve (at ~ 1 mm s^{-1} against ~ 10 mm s^{-1} for non-fat samples). Afterwards, depending on the content of starch or κCar, a peak or upward curve reaching a plateau could be observed within the first and second decades of sliding speed range. The high of the peaks (seen for samples ST(1)_κCar(0.3)_F(6), ST(3)_κCar(0.3)_F(6) and ST(2)_κCar(0.15)_F(3)) or plateau shape (ST(3)_κCar(0.0)_F(6) only) was not significantly different within samples (h = 0.03) and it represents an input of at least 30 % on the pre-determined CoF_{min} values.

In this study we hypothesize that the parameters CoF_i, CoF_{min} and CoF_{min} + h can be identified as boundary elements that delimit tribological regimes in fat-containing samples; except for sample ST(1)_κCar(0.0)_F(6) which presented visible fat lumps (causing inaccurate CoF measure, as per the large error bars) due to the absence of κCar and low concentration of starch. The tribological regimes were named as TR_1, TR_2 and TR_3 as indicated by **Fig. 7** and can be explained as follows:

- **TR_1**: this regime was characterized by a decreasing trend on CoF values from CoF_i to CoF_{min} as a result of selective entrainment of the fluid medium between the surfaces in contact (at this stage no particles are driven in the gap) (Gabriele, Spyropoulos & Norton, 2010). The lack of consistency on CoF measurement was associated to a transition period from dry-contact condition (static tribo-geometry) to the early stage of liquid entrainment.

- **TR_2**: this corresponds to the upward curve observed after CoF_{min} as the sliding speed further develops. The estimated 30 % augment in CoF_{min} (based on h value, see **Table 3**) was assigned to a gradual gel particles entrainment which was confirmed by CLSM images illustrated in next section for ST(2)_kCar(0.15)_F(3) friction experiment recorded at sliding speed of 2.5 mm s^{-1} (Gabriele, Spyropoulos & Norton, 2010).

- **TR_3**: the trend observed in TR_3 relies on the ability of the entrained material to accumulate on the surface of the static substrate. Different layers will be formed as the number of particles driven to the gap increases. As the thickness of the lubricant film is, at this stage, much larger than the size of an individual particle, friction and viscosity effects take place. The decay of CoF will rely on the ability of the multicomponent system to thicken the lubricant film (Liu, Stieger, van der Linden, & van de Velde, 2015). While formulations ST(1)_κCar(0.3)_F(6) and ST(3)_κCar(0.3)_F(6) depicted a decreasing CoF, for ST(3) _κCar(0.0)_F(6) CoF remained constant in TR_3. This suggests that the late release of the fat initially entrapped in very inner regions of the formed network by starch-κCar-milk proteins can contribute for a faster CoF decay.

3.4 Microstructure analysis

Figs. 8a to 8c illustrate magnified images (20 x) of skim milk colloidal suspension (control sample), ST(3)_κCar(0.0)_F(0) and ST(2)_κCar(0.15)_F(3) custards, respectively. **Fig. 8a** depicts a homogenous phase characteristic of dissolved skim milk powder. During the preparation of custard, pre-gelatinized starch is introduced to the system. In Figs. **8b and 8c,** it is possible to observe the microstructure starch granules with size ranging from 10 to 40 μm; which corroborates with the size distribution curves depicted by **Fig. 2**. **Fig. 8d** shows the CLSM image acquired for stained ST(2)_κCar(0.15)_F(3), prior to friction experiment, using fluorescence probes Nile Red, Fast Green, Calco-Fluor White and FITC to label, respectively, fat, protein, polysaccharide (in this case, κCar) and starch. Although FITC is a common probe used to bind starch, it has not effectively labeled starch in the sample tested. It can be suggested that the expected reactions between starch and probe were hindered by the network formed with gelatinized starch and casein. Hence, the black spaces shown in **Fig. 8d** were associated to the presence of gelatinized starch surrounded by a network composed of protein (pink colour) and κCar (blue colour).

Figure 8

Fig. 9 shows CLSM images obtained at different stages of the friction curve for ST(2)_κCar(0.15)_F(3). This sample was chosen because it presents all the proposed mechanisms of entrainment from low to high speeds. As observed by **Fig. 8d**, the microstructure of custard before the action of friction shows a network formed between protein (pink), starch (green) and κCar (blue) containing entrapped fat (red). At low speeds, the decay of CoF previously explained by the entrainment of liquid can be observed by the presence of all the labeled ingredients evenly distributed at the CLSM image recorded at 0.5 mm s^{-1}. The CLSM image acquired at 2.5 mm s^{-1}, where κCar and fat can be predominantly seen demonstrates an indicative of gel particles entrainment zone (TR_2). Upon application of friction, the entrained particles will have their structure disrupted and milk fat droplets which are non-polar by nature tend to move towards the hydrophobic sites of the 3M tape surface used to mimic tongue surface which is intrinsically hydrophobic but hydrophilic if coated with mucous fluid (Dresselhuis, Van Aken, De Hoog, & Cohen Stuart, 2008). Thus, decreasing and/or constant CoF regime (TR_3) takes place due to the accumulation of multilayers of material which favor the separation of the two rubbing surfaces. Evidences of multilayer deposition at high speeds can be observed by the CLSM image taken at 10 mm s^{-1}. This image clearly shows that the amount of protein and fat increased in comparison to the previous picture (2.5 mm s^{-1}). The increase of all labeled ingredients was assigned to the multilayer deposition at high speeds.

Figure 9

3.5 Sensory profiling of selected custard formulations

Table 6 shows that by using ranking test analysis, the selected samples were successfully differentiated in terms of thickness, stickiness, oiliness, creaminess and smoothness ($p<0.05$). Higher viscosity was perceived for ST(3)_κCar(0.3)_F(6), followed by ST(1)_κCar(0.3)_F(6), ST(2)_κCar(0.15)_F(3), ST(3)_κCar(0.0)_F(6) and ST(3)_κCar(0.0)_F(0). Exactly the same decreasing order of viscosities measured at a shear rate of 50 s^{-1} was observed; suggesting that this condition represented well the flow behavior of custard in the mouth during sensory rating. The perception of thickness was closely related to the presence of κCar, once no significant differences were observed by decreasing the amount of starch in the comparison between samples ST(1)_κCar(0.3)_F(6) and ST(3)_κCar(0.3)_F(6). Similarly, the effect of fat on the thickness attribute was neglected; as the difference rank sum within the products ST(3)_κCar(0.0)_F(0) and ST(3)_κCar(0.0)_F(6) was lower than 14.55 (value of LSD).

Table 6

As expected, samples presenting high ranking sum for the viscous attribute depicted the highest levels of stickiness. Stickiness, however, cannot be mainly characterized as a bulk-related sensory attribute. Surface-related features, such as, lubricant properties are likely to play an important role on the perception of stickiness.

Oiliness, creaminess and smoothness were only perceived upon variations in the fat content; as per comparison among samples ST(2)_κCar(0.15)_F(3), ST(3)_κCar(0.0)_F(0) and ST(3)_κCar(0.0)_F(6) (RS > 14.55). These are common attributes used to describe mouthfeel when food is confined to an extent that the shearing surfaces of tongue and palate interact (Selway & Stokes, 2013). As an example, De Wijk and collaborators have extensively studied the effect of fat content on creaminess and oiliness attributes of custard desserts. They have demonstrated that liberation of fat from starch matrix occurs when it is broken down by salivary amylase. Then free fat can migrate by convection currents to the surface of the food bolus acting as lubricant agent between the bolus and oral tissue (de Wijk, et al., 2007; de Wijk, et al., 2004; Engelen, et al., 2003). Aligned to saliva effect, entrainment speed also play important role on breaking down the gel microstructure of custard facilitating the transport of fat from inner-gel to regions near the surface where it can reduce friction. Our tribological study considered only the effect of entrainment speed on friction profile. In absence of saliva it was possible to observe influences exerted by κCar and starch on CoF which were associated to mechanisms of particle entrainment and interactions between product and substrate (3M tape). As it has been well reported by literature (Selway & Stokes, 2013; Laguna et al., 2017) the presence of saliva facilitates the food microstructure breaking down and it renders hydrophilic features to the intrinsically hydrophobic tongue surface. Hence, mechanisms of product entrainment between tongue and palate will deviate from that observed by the tribometer set-up which uses a substrate, with predominant hydrophobic sites, non-wetted by mucus fluid.

4. CONCLUSION

This study demonstrated that κCar played an important role in the flow and friction behavior of fat-containing custard formulations. However, no influences were observed in the friction profile upon addition of this hydrocolloid in free-fat formulations. This indicates that the mechanisms of product entrainment as the sliding speed increases are affected by adding κCar or even increasing the content of starch due to changes on the hydrophobic interactions between the tape and emulsified fat. Despite the friction profile has demonstrated sensitivity to the addition of κCar, no influences on surface-related attributes (e.g., oiliness, creaminess) was observed on sensory measurements of samples with and without κCar. This was attributed to the presence of saliva, during the real oral processing, facilitating the food microstructure breakdown and release of fat which, in turn, migrates to the surface of tongue and palate forming a lubricant film. Our present tribological study takes into consideration only the effects of sliding speed range, temperature and roughness of surface similar to that observed in the tongue; further studies will involve the addition of saliva in the tribological apparatus to achieve improved simulation of the mouth conditions. By understanding how hydrocolloids influences flow and friction behavior and its relation with sensory measurements much savings can be generated to industry.

Acknowledgements

The authors are thankful to Dr Shaun Walters from School of Biomedical Sciences (SBMS-UQ) for his support during the acquisition of CLSM images.

Funding Sources

This research was supported under Australian Research Council's Industrial Transformation Research Program (ITRP) funding scheme (project number IH120100005). The ARC Dairy Innovation Hub is a collaboration between The University of Melbourne, The University of Queensland and Dairy Innovation Australia Ltd.

REFERENCES

Chen, J., Liu, Z., & Prakash, S. (2014). Lubrication studies of fluid food using a simple experimental set up. *Food Hydrocolloids*.

Chiappin, S., Antonelli, G., Gatti, R., & De Palo, E. F. (2007). Saliva specimen: A new laboratory tool for diagnostic and basic investigation. *Clinica Chimica Acta, 383*(1-2), 30-40.

Chojnicka-Paszun, A., de Jongh, H. H. J., & de Kruif, C. G. (2012). Sensory perception and lubrication properties of milk: Influence of fat content. *International Dairy Journal, 26*(1), 15-22.

de Wijk, R. A., & Prinz, J. F. (2007). Fatty versus creamy sensations for custard desserts, white sauces, and mayonnaises. *Food Quality and Preference, 18*(4), 641-650.

de Wijk, R. A., Prinz, J. F., Engelen, L., & Weenen, H. (2004). The role of α-amylase in the perception of oral texture and flavour in custards. *Physiology & Behavior, 83*(1), 81-91.

Dresselhuis, D. M., Van Aken, G. A., De Hoog, E. H. A., & Cohen Stuart, M. A. (2008). Direct observation of adhesion and spreading of emulsion droplets at solid surfaces. *Soft Matter, 4*(5), 1079-1085.

Engelen, L., de Wijk, R. A., Prinz, J. F., Janssen, A. M., Weenen, H., & Bosman, F. (2003). The effect of oral and product temperature on the perception of flavor and texture attributes of semi-solids. *Appetite, 41*(3), 273-281.

Fernández Farrés, I., & Norton, I. T. (2015). The influence of co-solutes on tribology of agar fluid gels. *Food Hydrocolloids, 45*, 186-195.

Gabriele, A., Spyropoulos, F., & Norton, I. T. (2010). A conceptual model for fluid gel lubrication. *Soft Matter, 6*(17), 4205-4213.

Garrec, D. A., & Norton, I. T. (2013). Kappa carrageenan fluid gel material properties. Part 2: Tribology. *Food Hydrocolloids, 33*(1), 160-167.

Gohar, R., & Rahnejat, H. (2008). *Fundamentals of tribology*. London: Imperial College Press.

Laguna, L., Farrell, G., Bryant, M., Morina, A., & Sarkar, A. (2017). Relating rheology and tribology of commercial dairy colloids to sensory perception. *Food & Function, 8*(2), 563-573.

Lawless, H. T. (2010). *Sensory Evaluation of Food : Principles and Practices (2nd Edition)*. New York: New York, NY, USA: Springer New York.

Liu, K., Stieger, M., van der Linden, E., & van de Velde, F. (2015). Fat droplet characteristics affect rheological, tribological and sensory properties of food gels. *Food Hydrocolloids, 44*, 244-259.

Malone, M. E., Appelqvist, I. A. M., & Norton, I. T. (2003). Oral behaviour of food hydrocolloids and emulsions. Part 1. Lubrication and deposition considerations. *Food Hydrocolloids, 17*(6), 763-773.

Malvern-Instruments. (2007a). Mastersizer 2000 - User Manual. In). United Kingdom: Malvern Instruments.

Malvern-Instruments. (2007b). Sample dispersion and refractive index guide. In). United Kingdom: Malvern Instruments Ltd. 2007.

McCarthy, O. J. (2003). Liquid products and semi-solid products. In *Encyclopedia of Dairy Sciences* (pp. 2445-2456). Amsterdam: Academic Press.

Moakes, R. J. A., Sullo, A., & Norton, I. T. (2015). Preparation and characterisation of whey protein fluid gels: The effects of shear and thermal history. *Food Hydrocolloids, 45*, 227-235.

Nagaoka, S., Hirata, Y., Iwaki, H., Sakamoto, K., Takagi, M., & Amagasa, T. (2001). A Study of the Surface Roughness of Tongue Cancer and Leukoplakia Using a Non-contact Three-dimensional Curved Shape Measuring System. *Oral Medicine & Pathology, 6*(2), 85-90.

Necas, J., & Bartosikova, L. (2013). Carrageenan: A review. *Veterinarni Medicina, 58*(4), 187-205.

Nguyen, P. T. M., Bhandari, B., & Prakash, S. (2016). Tribological method to measure lubricating properties of dairy products. *Journal of Food Engineering, 168*, 27-34.

Nguyen, P. T. M., Nguyen, T. A. H., Bhandari, B., & Prakash, S. (2015). Comparison of solid substrates to differentiate the lubrication property of dairy fluids by tribological measurement. *Journal of Food Engineering*.

Pradal, C., & Stokes, J. R. (2016). Oral tribology: Bridging the gap between physical measurements and sensory experience. *Current Opinion in Food Science, 9*, 34-41.

Prakash, S., Tan, D. D. Y., & Chen, J. (2013). Applications of tribology in studying food oral processing and texture perception. *Food Research International, 54*(2), 1627-1635.

Ranc, H., Servais, C., Chauvy, P. F., Debaud, S., & Mischler, S. (2006). Effect of surface structure on frictional behaviour of a tongue/palate tribological system. *Tribology International, 39*(12), 1518-1526.

Richter, V. B., de Almeida, T. C. A., Prudencio, S. H., & de Toledo Benassi, M. (2010). Proposing a ranking descriptive sensory method. *Food Quality and Preference, 21*(6), 611-620.

Selway, N., & Stokes, J. R. (2013). Insights into the dynamics of oral lubrication and mouthfeel using soft tribology: Differentiating semi-fluid foods with similar rheology. *Food Research International, 54*(1), 423-431.

Shama, F., & Sherman, P. (1973). Identification of stimuli controlling the sensory evaluation of viscosity II. Oral Methods. *Journal of Texture Studies, 4*(1), 111-118.

Tarrega, A., & Costell, E. (2006). Effect of composition on the rheological behaviour and sensory properties of semisolid dairy dessert. *Food Hydrocolloids, 20*(6), 914-922.

Toker, O. S., Dogan, M., Caniyilmaz, E., Ersöz, N. B., & Kaya, Y. (2013). The Effects of Different Gums and Their Interactions on the Rheological Properties of a Dairy Dessert: A Mixture Design Approach. *Food and Bioprocess Technology, 6*(4), 896-908.

FIGURE CAPTIONS

Figure 1: Schematic illustration of the tribo-rheometer set up.

Figure 2: Particle size distribution for (a) ST1%_κCar(0.0)_F(0), (b) ST(2)_κCar(0.15)_F(3) and (c) ST(3)_κCar0.30%_F(6). The presented curves are representative of the average of triplicate experiments (error bars not shown).

Figure 3: Pareto's chart of standardized estimated effects of Starch, κCar and Fat content in the (a) particle volume mean diameter, $D_{4,3}$ and (b) apparent viscosity measured at 50 s^{-1} of shear rate, η_{50}.

Figure 4: Flow behavior of custard prepared at different compositions.

Figure 5: Storage modulus G' (circle symbols) and loss modulus G'' (square symbols) measured and plotted against angular frequency for custard formulations with various starch, κCar and fat concentrations.

Figure 6: Friction curves of free-fat custard formulations: (a) ST(1)_κCar(0.3)_F(0) & ST(1)_κCar(0.3)_F(6); (b) ST(1)_κCar(0.0)_F(0) & ST(1)_κCar(0.0)_F(6); (c) ST(3)_κCar(0.3)_F(0) & ST(3)_κCar(0.3)_F(6); and (d) ST(3)_κCar(0.0)_F(0) & ST(3)_κCar(0.0)_F(6). The presented curves are representative of the average of triplicate experiments (error bars are shown in grey colour).

Figure 7: Schematic representation of the friction profile depicted by non-fat and fat-containing custard formulations.

Figure 8: Light microscopy (LM) images (20 x) obtained for (a) skim milk powder colloidal suspension, (b) ST(3)_κCar(0.0)_F(0) and (c) ST(2)_κCar(0.15)_F(3) . Confocal Laser Scanning Microscopy (CLSM) image shown in (d) for ST(2)_κCar(0.15)_F(3). In the CLSM image, fat, protein and κCar are labelled, respectively, with red, pink and blue colours.

Figure 9: CLSM images obtained at different stages of the friction curve. In the CLSM images, fat, protein and κCar are labelled, respectively, with red, pink and blue colours. The scale bars are 100 μm.

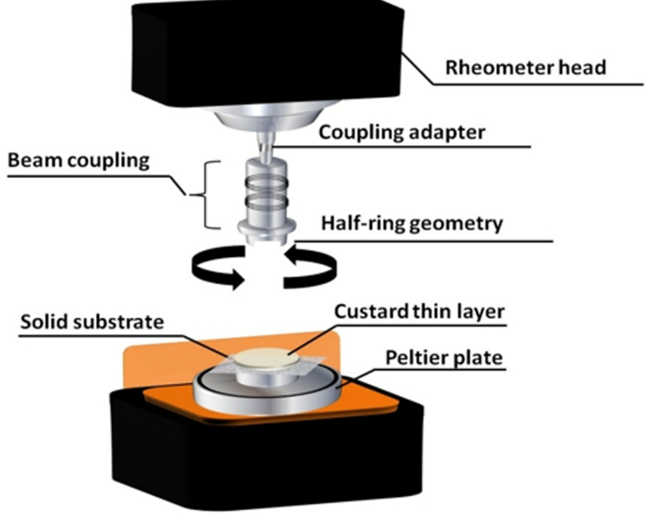
Rheometer head
Coupling adapter
Beam coupling
Half-ring geometry
Solid substrate
Custard thin layer
Peltier plate

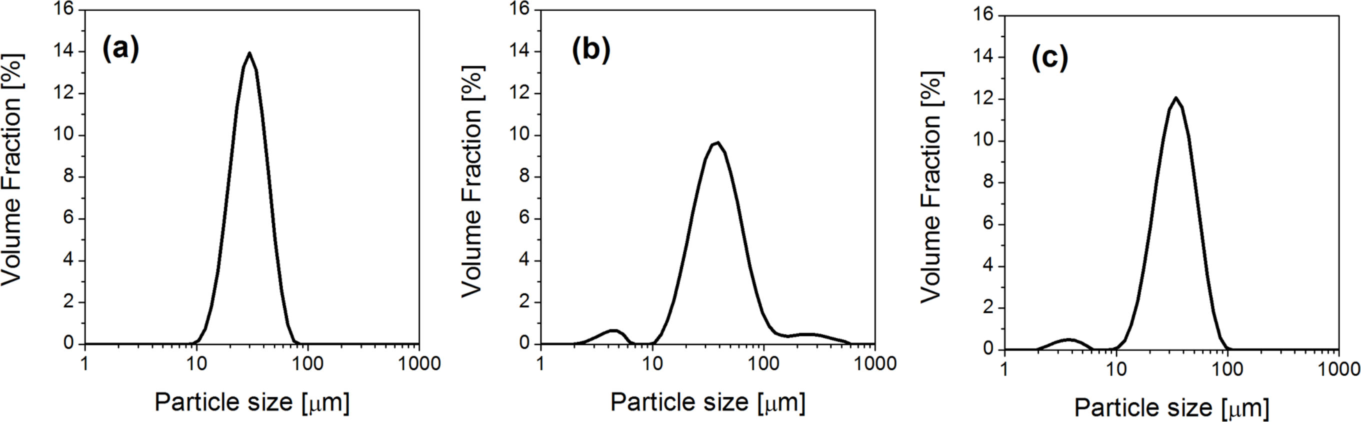
(a)
(b)
(c)
Volume Fraction [%]
Particle size [μm]
0
2
4
6
8
10
12
14
16
1
10
100
1000

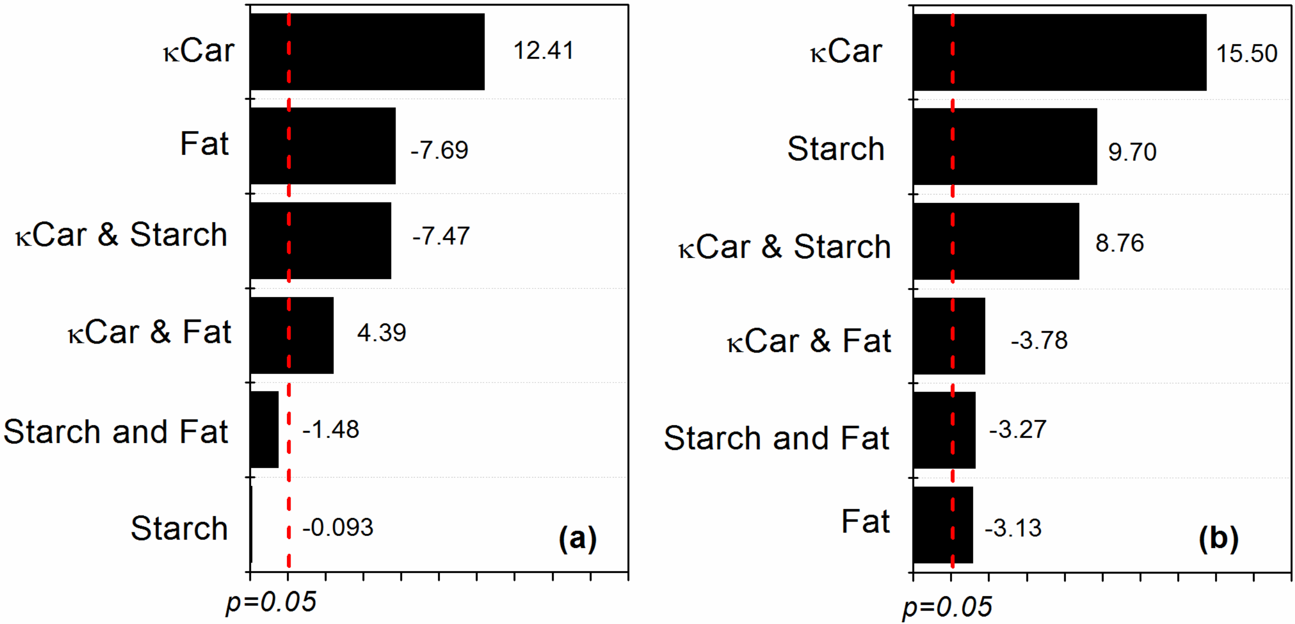
κCar
12.41
Fat
-7.69
κCar & Starch
-7.47
κCar & Fat
4.39
Starch and Fat
-1.48
Starch
-0.093
(a)
p=0.05
κCar
15.50
Starch
9.70
κCar & Starch
8.76
κCar & Fat
-3.78
Starch and Fat
-3.27
Fat
-3.13
(b)
p=0.05

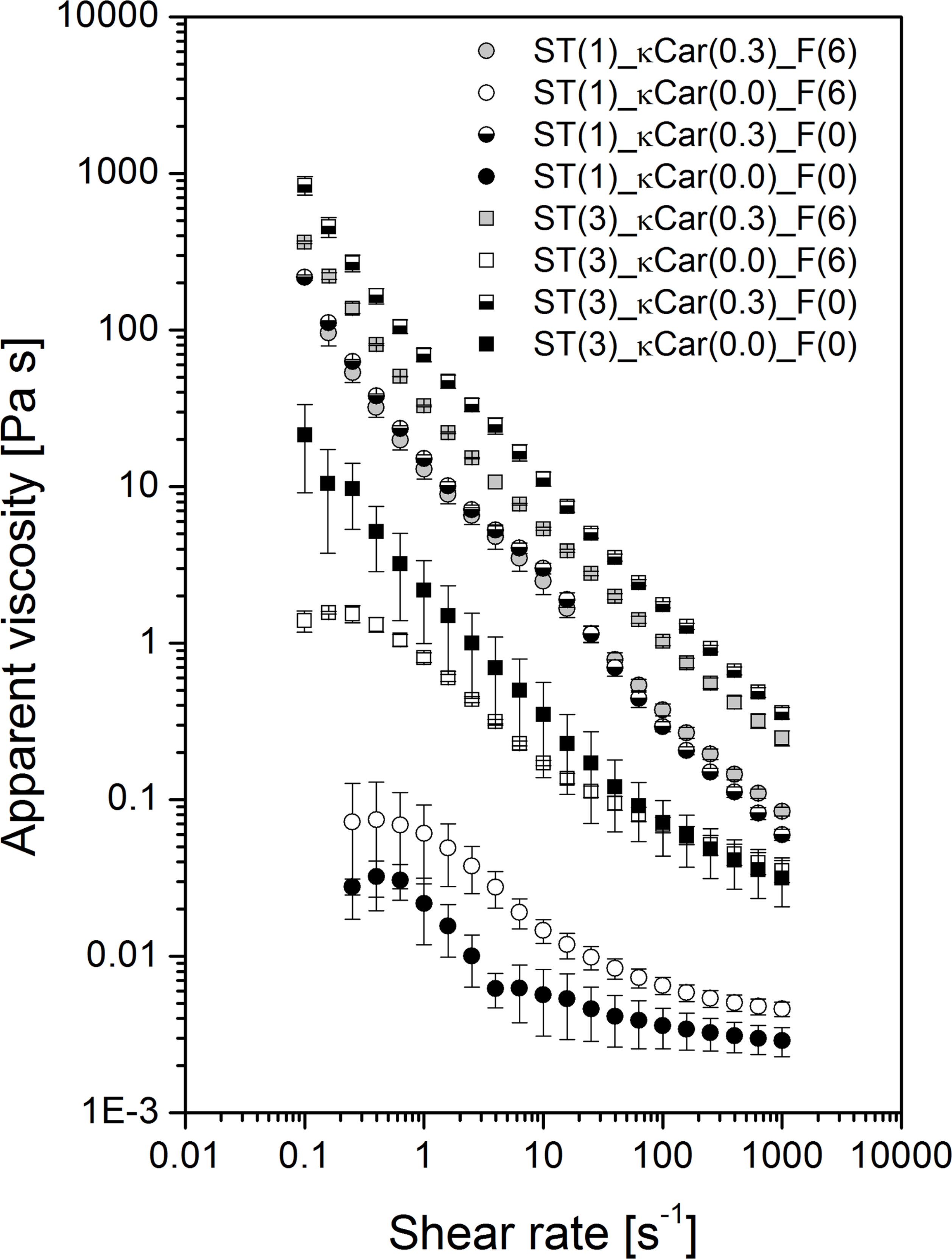
ST(1)_κCar(0.3)_F(6)
ST(1)_κCar(0.0)_F(6)
ST(1)_κCar(0.3)_F(0)
ST(1)_κCar(0.0)_F(0)
ST(3)_κCar(0.3)_F(6)
ST(3)_κCar(0.0)_F(6)
ST(3)_κCar(0.3)_F(0)
ST(3)_κCar(0.0)_F(0)
Apparent viscosity [Pa s]
Shear rate [s^-1]
10000
1000
100
10
1
0.1
0.01
1E-3
0.01
0.1
1
10
100
1000
10000

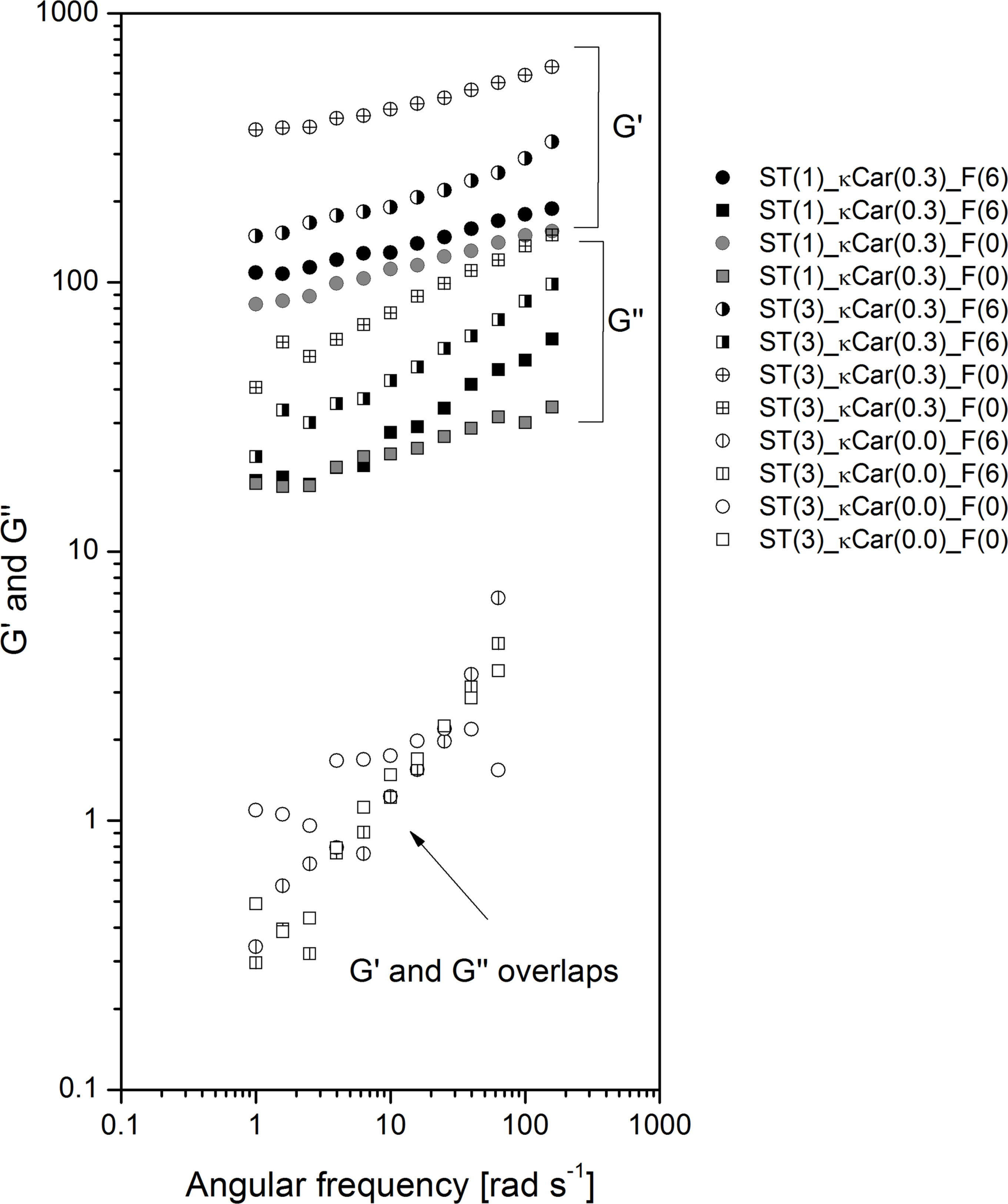

1000
100
10
1
0.1
G'
G''
G' and G''
G' and G'' overlaps
0.1
1
10
100
1000
Angular frequency [rad s-1]
ST(1)_κCar(0.3)_F(6)
ST(1)_κCar(0.3)_F(6)
ST(1)_κCar(0.3)_F(0)
ST(1)_κCar(0.3)_F(0)
ST(3)_κCar(0.3)_F(6)
ST(3)_κCar(0.3)_F(6)
ST(3)_κCar(0.3)_F(0)
ST(3)_κCar(0.3)_F(0)
ST(3)_κCar(0.0)_F(6)
ST(3)_κCar(0.0)_F(6)
ST(3)_κCar(0.0)_F(0)
ST(3)_κCar(0.0)_F(0)

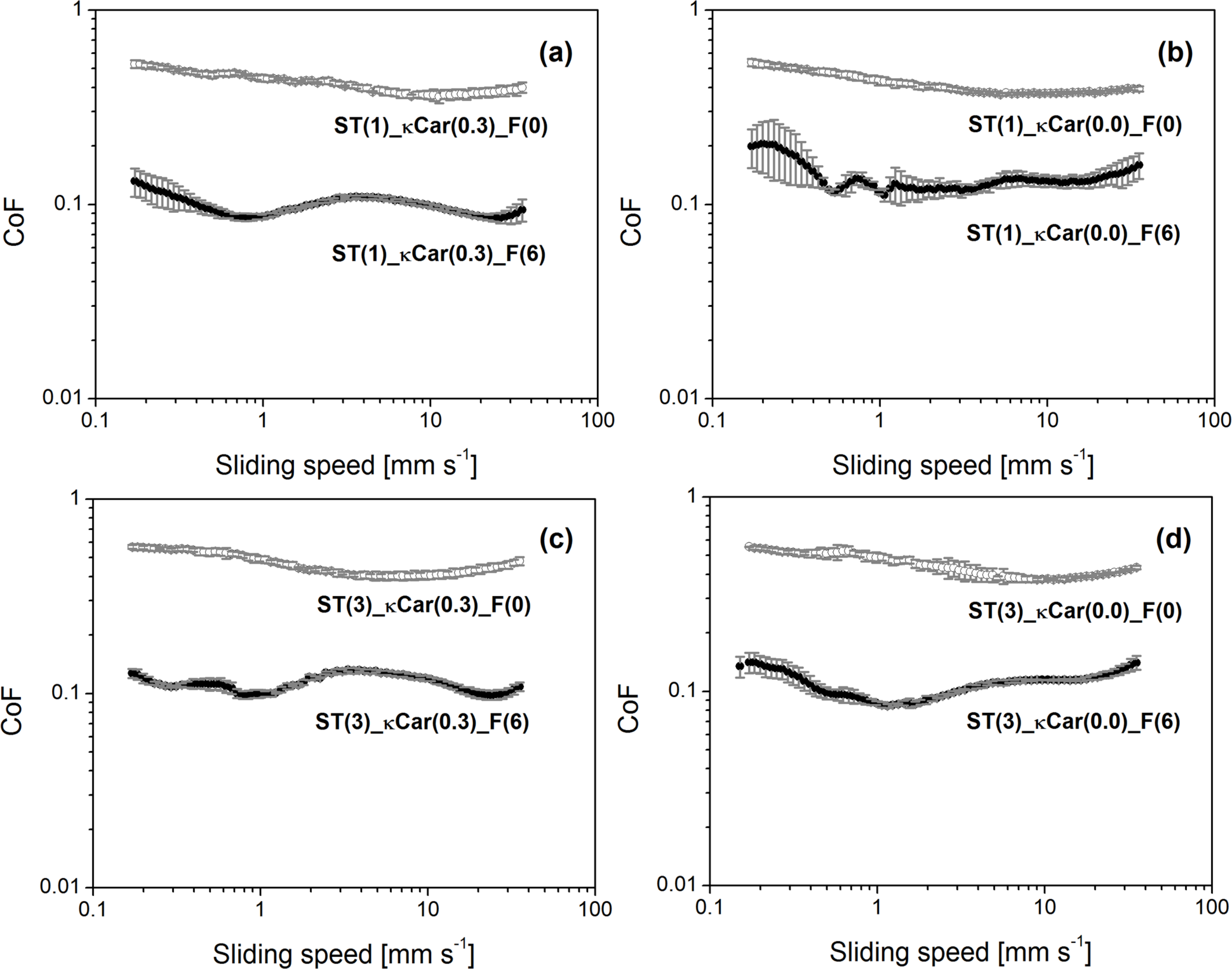

(a)
ST(1)_κCar(0.3)_F(0)
ST(1)_κCar(0.3)_F(6)
(b)
ST(1)_κCar(0.0)_F(0)
ST(1)_κCar(0.0)_F(6)
(c)
ST(3)_κCar(0.3)_F(0)
ST(3)_κCar(0.3)_F(6)
(d)
ST(3)_κCar(0.0)_F(0)
ST(3)_κCar(0.0)_F(6)
CoF
Sliding speed [mm s-1]

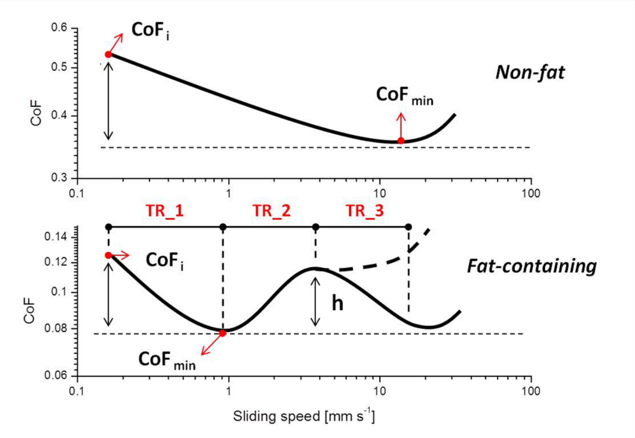

CoF_i
Non-fat
CoF_min
CoF
0.6
0.5
0.4
0.3
0.1
1
10
100
TR_1
TR_2
TR_3
0.14
0.12
0.1
0.08
0.06
CoF_i
Fat-containing
h
CoF_min
Sliding speed [mm s^-1]

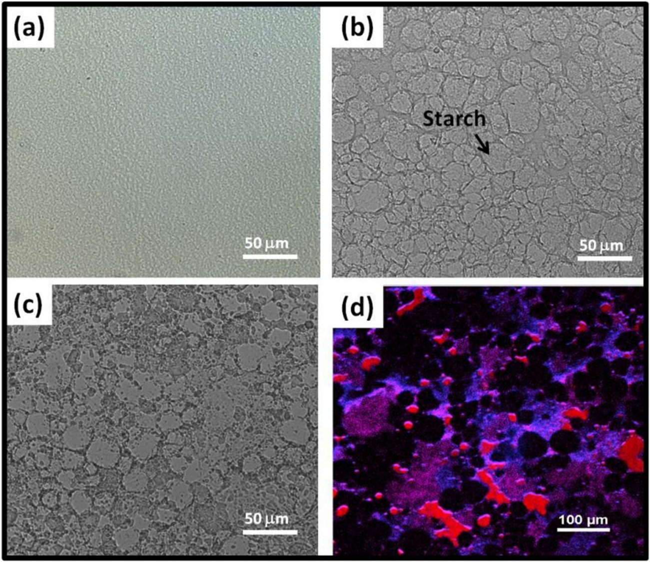
(a)
50 μm
(b)
Starch
50 μm
(c)
50 μm
(d)
100 μm

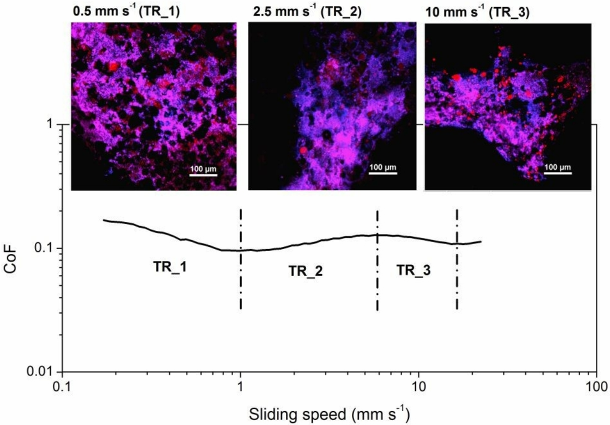

0.5 mm s⁻¹ (TR_1)
2.5 mm s⁻¹ (TR_2)
10 mm s⁻¹ (TR_3)
100 µm
100 µm
100 µm
CoF
1
0.1
0.01
TR_1
TR_2
TR_3
0.1
1
10
100
Sliding speed (mm s⁻¹)

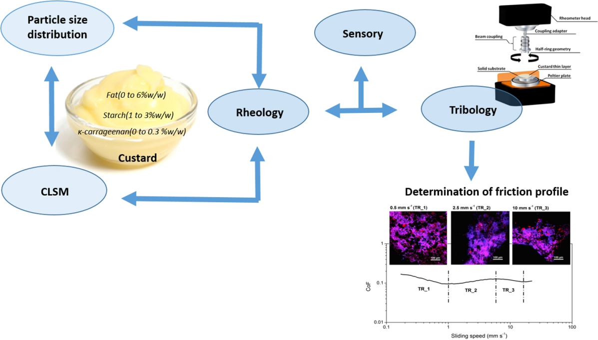

Particle size distribution
Sensory
Rheometer head
Coupling adapter
Beam coupling
Half-ring geometry
Solid substrate
Custard thin layer
Peltier plate
Fat(0 to 6%w/w)
Starch(1 to 3%w/w)
κ-carrageenan(0 to 0.3 %w/w)
Custard
Rheology
Tribology
CLSM
Determination of friction profile
0.5 mm s-1 (TR_1)
2.5 mm s-1 (TR_2)
10 mm s-1 (TR_3)
TR_1
TR_2
TR_3
CoF
Sliding speed (mm s-1)

TABLES

Table 1: Levels of the dependent variables (concentration of Starch, κCar and Fat, %w/w) of the factorial design with their respective designated nomenclature.

Nomenclature	Starch [% w/w]	κCar [%w/w]	Fat [%w/w]
ST(1)_κCar(0.0)_F(0)	1	0.0	0
ST(1)_κCar(0.3)_F(0)	1	0.3	0
ST(1)_κCar(0.0)_F(6)	1	0.0	6
ST(1)_κCar(0.3)_F(6)	1	0.3	6
ST(2)_κCar(0.15)_F(3)*	2	0.15	3
ST(3)_κCar(0.0)_F(0)*	3	0.0	0
ST(3)_κCar(0.3)_F(0)	3	0.3	0
ST(3)_κCar(0.0)_F(6)*	3	0.0	6
ST(3)_κCar(0.3)_F(6)*	3	0.3	6

**Asterisk symbols indicate samples chosen to perform sensory analysis.*

Table 2: Definitions of the textural attributes.

Attributes	**Definitions**
Thickness	Resistance to flow in the mouth
Smoothness	Perception of smoothness in the mouth from smooth to rough
Powderiness	The feeling of some particles and a chalky sensation in the mouth
Creaminess	The perception of 'oiliness' in the mouth and the degree of mouth coating. Usually, creaminess is perceived only when a certain viscosity threshold is reached.
Oiliness	Perception of the amount of fat in the sample

Table 3: $D_{4,3}$, η_{50}, CoF_i, CoF_{min} and h measured for the custard samples at conditions proposed by the factorial design.

Samples	**$D_{4,3}$ [μm]***	**η_{50} [Pa s]****	**CoF_i*****	**CoF_{min}*****	***h*******
ST(1)_κCar(0.0)_F(0)	33.1 ± 0.2[e]	0.0041±0.0015[d]	0.54 ± 0.02[a]	0.38 ± 0.01[a]	NA
ST(1)_κCar(0.0)_F(6)	27.9 ± 0.9[g]	0.0083±0.0012[d]	0.20 ± 0.04[b]	0.12 ± 0.01[b]	NA
ST(1)_κCar(0.3)_F(0)	37.5 ± 0.2[a,b]	0.698±0.083[c]	0.53 ± 0.02[a]	0.41 ± 0.02[a]	NA
ST(1)_κCar(0.3)_F(6)	38.2 ± 0.3[a]	0.785±0.085[c]	0.13 ± 0.02[c]	0.11 ± 0.00[b]	0.03 ± 0.00[a]
ST(3)_κCar(0.0)_F(0)	35.0 ± 0.1[d]	0.121±0.058[d]	0.55 ± 0.00[a]	0.42 ± 0.05[a]	NA
ST(3)_κCar(0.0)_F(6)	31.5 ± 0.3[f]	0.0951±0.0093[d]	0.14 ± 0.02[b,c]	0.10 ± 0.00[b]	0.03 ± 0.00[a]
ST(3)_κCar(0.3)_F(0)	36.6 ± 0.2[b,c]	3.52±0.19[a]	0.57 ± 0.01[a]	0.41 ± 0.01[a]	NA
ST(3)_κCar(0.3)_F(6)	33.6 ± 0.7[e]	1.988±0.088[b]	0.13 ± 0.01[c]	0.13 ± 0.00[b]	0.03 ± 0.00[a]
ST(2)_κCar(0.15)_F(3)	35.5 ± 0.1[c,d]	0.594±0.037[c]	0.17 ± 0.01[b,c]	0.12 ± 0.01[b]	0.04 ± 0.01[a]

**Values within a column not sharing a common superscript are significantly different (p-value<0.05, Tukey test).*

**$D_{4,3}$ express the particle volume mean diameter*

*** η_{50} is the apparent viscosity measured at 50 s^{-1} shear rate.*

**** CoF_i, CoF_{min} and h are friction parameters corresponding to, respectively, CoF measured at 0.15 mm s^{-1}, minimum CoF and peak height from the baseline built at CoF_{min}.*

Table 4: Tangent loss (tan δ) of selected custard formulations showing gel-like behavior.

Samples	tan δ
ST(3)_κCar(0.0)_F(0)	0.92 ± 0.21^{a}
ST(3)_κCar(0.0)_F(6)	0.99 ± 0.12^{a}
ST(2)_κCar(0.15)_F(3)	0.23 ± 0.02^{b}
ST(1)_κCar(0.3)_F(0)	0.21 ± 0.01^{b}
ST(1)_κCar(0.3)_F(6)	0.22 ± 0.02^{b}
ST(3)_κCar(0.3)_F(6)	0.23 ± 0.03^{b}
ST(3)_κCar(0.3)_F(0)	0.18 ± 0.01^{b}

**Values within a column not sharing a common superscript are significantly different (p-value<0.05, Tukey test).*

Table 5: Contact angle of ethanol and water sessile drop measured on the surface of the 3M tape.

Liquid	Contact angle
Water	97.4 ± 0.2^{a}
Ethanol	44.2 ± 0.1^{b}

**Values within a column not sharing a common superscript are significantly different (p-value<0.05, Tukey test).*

Table 6: Rank sum of selected sensory attributes obtained for samples ST(1)_κCar(0.3)_F(6), ST(2)_κCar(0.15)_F(3), ST(3)_κCar(0.0)_F(0), ST(3)_κCar(0.0)_F(6) and ST(3)_κCar(0.3)_F(6).

	Rank sum (RS)						
	Viscous	**Sticky**	**Oily**	**Creamy**	**Smooth**	**Powdery**	**Astringency**
ST(1)_κCar(0.3)_F(6)	43	40	39.5	38.5	36.5	43	37.5
ST(2)_κCar(0.15)_F(3)	33.5	31	33.5	41.5	40	37	36
ST(3)_κCar(0.0)_F(0)	11	11	11	14	19.5	27	32
ST(3)_κCar(0.0)_F(6)	22.5	28	36	39	39.5	26	32.5
ST(3)_κCar(0.3)_F(6)	55	55	45	32	29.5	32	27
p-value	p<0.001	p<0.001	p<0.001	0.001	0.028	0.119	0.659